Transcription control by the ENL YEATS domain in acute leukemia

Published in final edited form as:

Nature. 2017 March 09; 543(7644): 270–274. doi:10.1038/nature21688.

Transcription control by the ENL YEATS domain in acute leukemia

Michael A. Erb[1], **Thomas G. Scott**[1], **Bin E. Li**[2,3,4], **Huafeng Xie**[2,3,4], **Joshiawa Paulk**[1], **Hyuk-Soo Seo**[5], **Amanda Souza**[1], **Justin M. Roberts**[1], **Shiva Dastjerdi**[1], **Dennis L. Buckley**[1], **Neville E. Sanjana**[6,7], **Ophir Shalem**[6,7], **Behnam Nabet**[1], **Rhamy Zeid**[1], **Nana K. Offei-Addo**[5], **Sirano Dhe-Paganon**[5], **Feng Zhang**[6,7], **Stuart H. Orkin**[2,3,4,8], **Georg E. Winter**[1,9], and **James E. Bradner**[1,10,11,*]

[1]Department of Medical Oncology, Dana-Farber Cancer Institute, Boston, MA

[2]Division of Hematology/Oncology, Boston Children's Hospital, Boston, MA

[3]Department of Pediatric Oncology, Dana-Farber Cancer Institute, Boston, MA

[4]Harvard Stem Cell Institute, Harvard Medical School, Boston, MA

[5]Department of Cancer Biology, Dana-Farber Cancer Institute, Boston, MA

[6]Broad Institute, 7 Cambridge Center, Cambridge, MA 02142, USA

[7]McGovern Institute for Brain Research, Department of Brain and Cognitive Sciences, Department of Biological Engineering, Massachusetts Institute of Technology, Cambridge, MA 02139, USA

[8]Howard Hughes Medical Institute, Boston Children's Hospital, Boston MA

[10]Department of Medicine, Harvard Medical School, Boston, MA

Abstract

Correspondence may be addressed to: James E. Bradner, MD, Novartis Institutes of BioMedical Research, 181 Massachusetts Avenue, Cambridge, MA 02139, james.bradner@novartis.com.

[9]Present address: Research Center for Molecular Medicine of the Austrian Academy of Sciences, Vienna, Austria

[11]Present address: Novartis Institutes for BioMedical Research, Cambridge, MA

SUPPLEMENTARY INFORMATION is available in the online version of the paper.

AUTHOR CONTRIBUTIONS

M.A.E. performed experiments and analyzed data. G.E.W. designed plasmids for the dTAG system with J.M.R. and performed CRISPR-Cas9 screens collaboratively with N.E.S., O.S., and F.Z. T.G.S. assisted cellular assays. B.E.L., H.X., and S.H.O. performed experiments on HSPCs. J.P., H.-S.S., N.K.O.-A., and S.D.P. performed protein biochemistry. A.S. performed mouse experiments. S.D. and D.L.B. designed and synthesized dTAG molecules. B.N. assisted in sgRNA validation. R.Z. assisted in exon-scanning CRISPR-Cas9. M.A.E., G.E.W., and J.E.B. designed the experimental strategy and wrote the manuscript.

AUTHOR INFORMATION

The ChIP-seq and RNA-seq data featured in this publication can be accessed online using the GEO Publication Reference ID GSE82118.

The authors declare competing financial interests: J.E.B. is now an employee, shareholder, and executive of Novartis Pharmaceuticals; G.E.W. is a consultant for C4 Therapeutics; and N.E.S., O.S., and F.Z. are inventors on a patent application related to CRISPR screening technology.

Recurrent chromosomal translocations involving the *mixed lineage leukemia* gene (*MLL*) give rise to a highly aggressive acute leukemia associated with poor clinical outcome[1]. The preferential involvement of chromatin-associated factors in MLL rearrangement belies a dependency on transcription control[2]. Despite recent progress made in targeting chromatin regulators in cancer[3], available therapies for this well-characterized disease remain inadequate, prompting the present effort to qualify new targets for therapeutic intervention. Using unbiased, emerging CRISPR-Cas9 technology to perform a genome-scale loss-of-function screen in MLL-AF4-positive acute leukemia, we identified *ENL* (*eleven-nineteen leukemia*) as an unrecognized dependency particularly indispensable for proliferation *in vitro* and *in vivo*. To explain the mechanistic role for ENL in leukemia pathogenesis and dynamic transcription control, we pursued a chemical genetic strategy utilizing targeted protein degradation. Acute ENL loss suppresses transcription initiation and elongation genome-wide, with pronounced effects at genes featuring disproportionate ENL load. Importantly, ENL-dependent leukemic growth was contingent upon an intact YEATS chromatin reader domain. These findings reveal a novel dependency in acute leukemia and a first mechanistic rational for disrupting the YEATS domain in disease.

Our group has longitudinally studied and targeted oncogenic transcription via disruption of chromatin-dependent signaling between oncogenic transcription factors and RNA polymerase (Pol) II. Previously, we collaboratively reported the function of acetyl-lysine binding factors, the BET bromodomain proteins (BRD2, BRD3, and BRD4), in enhancer-mediated transcription control of oncogenic *MYC* in hematologic malignancies[4,5], notably including MLL[6]. In MLL, aberrant chromatin structure is a hallmark feature that has been the focus of coordinated drug discovery efforts[7–12]. Despite recent progress, these rearrangements still portend a poor prognosis requiring immediate intervention leveraging to high-risk protocols[1], thus motivating our effort to illuminate new cancer-specific dependencies in MLL.

We undertook a genome-scale CRISPR/Cas9 knockout (GeCKO[13]) screen in the well-studied and MLL-AF4 rearranged human acute myeloid leukemia (AML) cell line, MV4;11 (Fig. 1a, Extended Data Fig. 1a, and Supplementary Table 1). Changes in sgRNA abundance after 15 days of culturing was quantified by massively parallel DNA sequencing and analyzed by RIGER[14], revealing several known MLL drivers (*FLT3-ITD*, *HOXA9*, and *MEIS1*) and essential genes (*RPL9*, *GAPDH*, *ATP5B*, and *CDC23*) as critical to proliferation[1,15,16]. Interestingly, sgRNAs targeting the YEATS (Yaf9, ENL, AF9, Taf14, Sas5) domain-containing *ENL* gene (also known as *MLLT1*) were among the most highly depleted, which given recent elucidation of the YEATS domain as a novel acyl-lysine reader module[17–20], prompted further investigation. ENL has been implicated in transcription control as a core component of the super elongation complex (SEC)[21–25], which also includes the positive transcription elongation factor b (P-TEFb) heterodimer (CDK9 and CyclinT1). ENL has also been suggested to interact directly with DOT1L[21,22,23], a critical and selective requirement in *MLL*-fusion leukemia[7,9,11,12], altogether supporting a rationale for ENL in MLL pathogenesis.

In order to validate *ENL* as a growth requirement, four additional sgRNAs were designed (Fig. 1b) and tested alongside the *ENL*-targeted sequence most highly depleted in the initial

screen (sgENL_e1). Each was confirmed to mediate on-target Cas9 activity against *ENL* (Extended Data Fig. 1b), inhibiting competitive growth of MV4;11 cells similarly to loss of FLT3 (Fig. 1c and Extended Data Fig. 1c, d), a *bona fide* target in the *FLT3-ITD*-positive cell line[15]. Of the 7 additional cell lines tested, each of which comparably express ENL, (Extended Data Fig. 1e), the SEMK2 (*MLL-AF4* ALL), OCI/AML-2 (*MLL-AF6* AML), MOLM-13 (*MLL-AF9* AML), NOMO-1 (*MLL-AF9* AML), and SKM-1 (*MLL* wild-type AML) cell lines were sensitive to ENL loss, while only HL-60 (*MLL* wild-type AML) and JURKAT (T-ALL) were not (Fig. 1d, e and Extended Data Fig. 1f–j). Additionally, an MV4;11 xenotransplantation model of disseminated leukemia in mice was sensitive to *ENL* loss, exhibiting marked reductions in disease progression and an overall survival benefit with CRISPR/Cas9 targeting (Fig. 1f–h). In contrast, competitive growth assays revealed that proliferation of lineage^{-}, *Sca*1^{+}, c-*Kit*$^{+}$ (LSK) murine hematopoietic progenitors was minimally affected by *Enl* loss (Fig. 1i, Extended Data Fig. 2a, b), qualifying ENL for further consideration as a leukemia target. Interestingly, but consistent with the initial GeCKO screen results, loss of the highly homologous YEATS-containing protein, AF9, had no observable anti-proliferative effects in MV4;11 or MOLM-13 cells (Extended Data Fig. 1l), suggesting a specific, unique requirement for ENL function in acute leukemia.

Given the previous annotation of *ENL* as a transcriptional activator[21–25], we hypothesized that ENL supports the pathogenesis of acute leukemia via maintenance of dysregulated gene expression. To test this, we employed a novel functional genetic strategy, building upon phthalimide conjugation of small molecules as an approach to achieve targeted protein degradation[26]. Using FKBP12^{F36V} as a protein tag for ENL, a hetero-bifunctional small molecule selectively targeting FKBP12^{F36V} and the E3 ubiquitin ligase, CRBN, induces degradation of the ENL chimera. Conveniently, the previously identified F36V mutation produces a “hole” in the protein surface that accommodates a complementary steric “bump” on the ligand[27], thereby avoiding targeting of FKBP12^{WT}.

With a hemagglutinin (HA) epitope tag used for detection, ENL was expressed as amino and carboxy terminal FKBP12^{F36V} fusions in MV4;11-Cas9 cells and efficiently degraded at nanomolar concentrations by both dTAG-7 and dTAG-13 (Fig. 2a and Extended Data Fig. 3a–d), notably within 30 min or 1 hour, respectively (Fig. 2b and Extended Data Fig. 3e). This system proved amenable for use in multiple cellular systems (Extended Data Fig. 3f–h) and durable over multiple days following a single treatment (Extended Data Fig. 3i, j), particularly with dTAG-13 treatment, which led to its selection for further characterization. Upon selective inactivation of endogenous *ENL* and clonal expansion of lines bearing N- and C-terminal fusions (Extended Data Fig. 4a, b), expression proteomics revealed exclusive loss of ENL with a single 3 hour dTAG-13 exposure (Fig. 2c) while FKBP12^{WT} is spared by this “bump-hole” strategy.

Administration of dTAG produced dose-responsive decreases in viability and potently suppressed proliferation in the absence of endogenous ENL (Fig. 2d and Extended Data Fig. 4c–f), with undetectable effects in wild-type MV4;11 cells (Extended Data Fig. 4g, h). We focused subsequent analyses on the C-terminally tagged MV4;11 cell line (Cas9+, ENL-FKBP12^{F36V}-HA+, ENL$^{-/-}$) as it featured a doubling time (31.3 hr, least-squares nonlinear regression, $R^2 = 0.956$) closer to that of wild-type MV4;11 (25.8 hr, $R^2 = 0.994$) than did the

N-terminally tagged line (35.0 hr, $R^2 = 0.995$). BrdU staining revealed that growth impairment downstream of pharmacologic ENL degradation can be attributed to rapid induction of G1 arrest and an accumulation of sub-G1 cells over 72 hours (Fig. 2e and Extended Data Fig. 4i). Consistent with prior annotations of ENL as a transcriptional activator, we observed subtle loss of gene expression by cell-count normalized RNA-seq at 8 hours, followed by global downregulation of active transcripts at 24 and 96 hours (Fig. 2f). We noted that several well-characterized leukemic drivers, including *HOXA10*, *MYC*, *MYB*, and *MEIS1* were among the earliest and most severely downregulated transcripts, while the myeloid differentiation marker *ITGAM* (CD11b/MAC-1), was contrastingly upregulated (Fig. 2g). Underlying global transcriptional defects at 24 hours was a concomitant decrease in RNA Pol II abundance at transcription start sites (TSS) and gene bodies of active genes (Fig. 2h, i).

By chromatin immunoprecipitation and next-generation DNA sequencing (ChIP-seq), we found ENL-FKBP12^{F36V} genomic localization (using HA-directed antibody) in MV4;11 (Cas9+, ENL-FKBP12^{F36V}-HA, ENL$^{-/-}$) cells to be closely correlated with wild-type ENL in the parental MV4;11 cells (Extended Data Fig. 5a), with each factor preferentially enriched at TSS (Fig. 3a and Extended Data Fig. 5b, c). Enrichment also correlated with epigenomic localization of reported YEATS domain substrates[17–20], H3K9ac, H3K18ac, and H3K27ac (Extended Data Fig. 5d–i). Interestingly, ranking ENL-bound loci uncovered an asymmetric distribution of ENL on the genome whereby a small fraction (ENL: 4.0%; ENL-FKBP: 2.5%) of all bound sites were enriched for a disproportionate amount of total ENL (ENL: 51.2%; ENL-FKBP: 50.1%) (Fig. 3b, c and Extended Data Fig. 5j). Within the set of asymmetrically loaded targets, we identified a large number of leukemogenic genes such as *MYC*, *MYB*, *HOXA10*, and *MEIS1*. A similar phenomenon was observed in MOLM-13 cells with preferential localization of ENL to promoters (Extended Data Fig. 6a), notably correlated to H3K27ac enrichment (Extended Data Fig. 6b; GEO ID: GSM1652920[28]) and asymmetrically distributed on the genome (Extended Data Fig. 6c, d).

By integrating these gene sets with kinetic gene expression profiling following dTAG-13 exposure, we uncovered preferential downregulation of asymmetrically enriched ENL target genes (Fig. 3d and Extended Data Fig. 7a–c), prompting further interrogation of class-specific RNA Pol II dynamics at ENL target genes. By ChIP-seq with cell-count normalization (ChIP-Rx), we uncovered preferential loss of RNA Pol II from the gene bodies of asymmetrically loaded targets, but with comparatively minimal effects at their TSS, reflecting a pause release defect at those genes (Fig. 3e and Extended Data 7d, e). Given previous characterization of ENL as a member of the SEC, we reasoned these effects might be consequences of SEC recruitment to chromatin. To test this, we focused on the chromatin localization of AFF4 and CDK9, which are scaffolding and catalytic subunits of the SEC, respectively. Following a 6-hour treatment with dTAG-13, we uncovered an evident loss of AFF4 from promoters of asymmetrically, but not typically, loaded targets (Fig. 3f, h, i and Extended Data Fig. 7f, i), which was accompanied also by a preferential loss of CDK9 from the promoters of those genes (Fig. 3g–i and Extended Data Fig. 7g, i). This suggested that ENL may contribute to recruitment of the SEC to asymmetrically loaded target genes to promote productive elongation. To test this, we focused on the catalytic output of CDK9 activity (phosphorylation of Ser2 of the RNA Pol II C-terminal domain heptapeptide repeat)

as a marker of elongating polymerase[31]. Following 24 hours of dTAG-13 treatment, we observe diminished pSer2-RNA Pol II enrichment specifically within gene bodies of ENL targets with asymmetric enrichment (Fig. 3h, i and Extended Data Fig. 7h, i).

As ENL has been reported to bind directly to DOT1L[21,22,23], we explored the functional relationship between these two factors. The rapid anti-proliferative response to ENL destabilization suggests a mechanism distinct from DOT1L function, as both genetic and chemical targeting of DOT1L is characterized by a delayed (7-10 day) effect on MLL growth and viability[7,9]. Indeed, bulk levels of H3K79me2 were minimally changed by ENL degradation and only modest effects on locus-specific H3K79me2 were observed at asymmetric ENL target genes by ChIP-seq (Extended Data Fig. 8a–c). As any changes to H3K79me2 occur several days after the first gene-expression changes occur following ENL degradation (96 hours versus 6 hours), we interpret these effects as secondary events attributable to the effect of ENL loss. To further dissect DOT1L-independent and DOT1L-dependent ENL phenotypes, we leveraged the rapid kinetics afforded by the dTAG/ENL system, finding that cell cycle and gene expression effects following ENL degradation were antecedent to those induced by DOT1L inhibition (Extended Data Fig. 8d, e). Moreover, combination treatments for 96 hours revealed an additive effect on the suppression of *MYC* and *HOXA9* transcription compared to either single agent treatment (Extended Data Fig. 8f). Also, while we were able to reproduce previous reports that DOT1L inhibition specifically downregulates MLL fusion target genes[7,9], we did not uncover preferential suppression of published MLL-AF4 target genes following dTAG-13 treatment, and MLL-AF4 target genes exhibit minimal overlap with asymmetrically loaded ENL targets (Extended Data Fig. 8g–i)[10,29]. Together, these data support that ENL degradation produces anti-leukemic effects on gene expression that occur, at least in part, through DOT1L-independent mechanisms. This agrees with the apparent ENL requirement in MLL^{WT} acute leukemia (Extended Data Fig. 1h), whereas DOT1L is selectively required in MLL-rearranged leukemia[7,9].

Given the evident addiction to ENL in acute leukemia cells, we employed saturating CRISPR-Cas9 mutagenesis to aid in the qualification of functionally relevant protein domains for drug discovery efforts[30]. We observed strong negative selection from sgRNAs targeting all annotated regions of ENL, with no regions emerging as a clear outlier (Fig. 4a). Given the sensitivity of CRISPR-Cas9 directed at the YEATS domain, and our positive experience approaching acetyl-lysine recognition motifs with discovery chemistry, we explored whether ENL-dependent growth was contingent on YEATS domain function. Informed by published structure-function studies of the highly homologous AF9[17], we engineered ENL mutations predicted to either minimally or severely affect acetyl-lysine recognition by featuring alanine replacements at Phe47 or Tyr78, respectively (Extended Data Fig. 9a). As previously reported for AF9, we confirmed the ability of wild-type ENL to bind H3K9ac and H3K27ac, and that while this interaction was moderately affected by mutation of Phe47 to alanine, ENL^{Y78A} exhibited a nearly complete inability to bind acetyl-lysine (Fig. 4b and Extended Data Fig. 9b–d). Despite equivalent expression, unaffected nuclear localization, and confirmed thermal stability in MV4;11-Cas9 cells (Extended Data Fig. 9e–h), ENL^{F47A} and ENL^{Y78A} exhibited moderate and severe defects in the localization to chromatin, respectively (Fig. 4c–e). Ultimately, these findings tracked with the ability of

each construct to rescue loss of endogenous ENL (Fig. 4f), providing genetic validation of the YEATS domain as a functional, emerging therapeutic target in leukemia.

In advance of identifying direct-acting inhibitors of ENL, we present data in support of a facile chemical biology platform to study dynamic cellular processes. We anticipate broad applicability of this technology beyond the scope of this study. We use the dTAG system to study the “fast biology” of transcription activation and elongation, capable of disentangling immediate versus secondary effects, complementing if not improving genetic perturbations (e.g. siRNA, CRISPR). Together, these studies provide support for a DOT1L-independent mechanism of leukemic maintenance, in which ENL recruitment of the SEC to promoters contributes to transactivation of as-yet undruggable oncogenes, such as *MYC*, *MYB*, and *HOXA10*. Importantly, whereas the role of *ENL* as a frequent fusion partner of *MLL* in leukemia has been known[1], we report wild-type ENL, and specifically its YEATS domain, as an unrecognized cancer-specific dependency in acute leukemia. We and others may now pursue the discovery of chromatin-competitive antagonists of the ENL YEATS domain, with mechanistic guidance, as leukemia therapy.

Extended Data

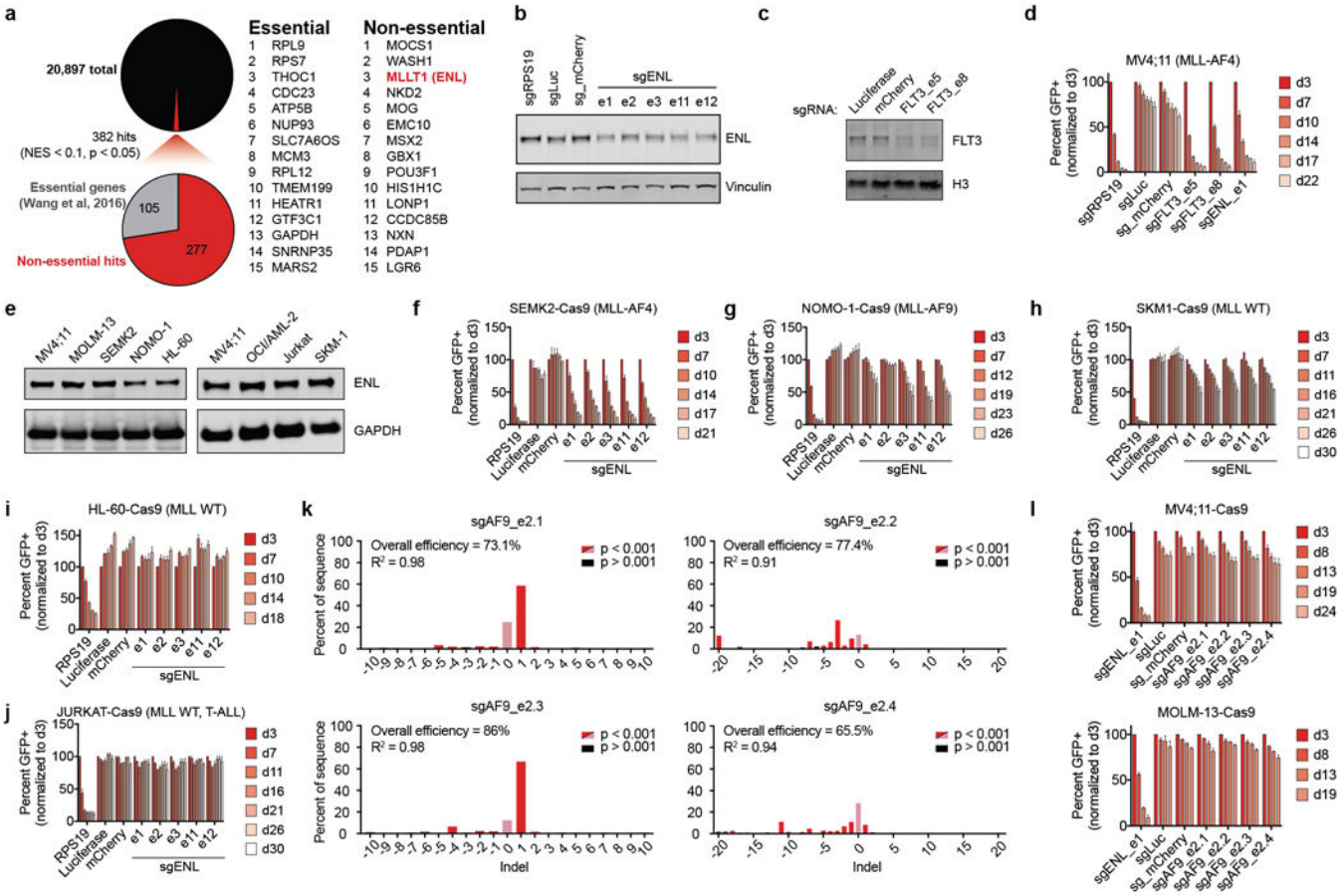

Extended Data Figure 1.

(a) Summary of GeCKOv2 screen results in MV4;11 cells showing the number of hits (NES < 0.1 and p < 0.05 in both replicates) and the percentage of hits known to be essential genes. Right: Top fifteen hits in essential and non-essential protein-coding genes.
(b) Immunoblot of ENL 5 days after transduction with the indicated sgRNA.
(c) Immunoblot of FLT3 5 days after transduction with the indicated sgRNA.
(d) Competition-based CRISPR-Cas9 mutagenesis in MV4;11-Cas9 cells. Percent GFP+ subpopulation (sgRNA-positive) after transduction with lentiviral constructs co-expressing GFP and an sgRNA indicated. Mean ± s.d., $n = 3$.
(e) ENL protein expression by immunoblot of all cell lines tested for ENL-dependent growth.
(f–j) Same as in (d) for the cell lines and sgRNAs indicated.
(k) Indel quantification by TIDE (tracking of indels by sequence trace decomposition) analysis 5 days after transduction with the sgRNA indicated in MV4;11-Cas9 cells.
(l) Same as in (d) for the cell lines and sgRNAs indicated, $n = 4$ for MV4;11, $n = 3$ for MOLM-13.

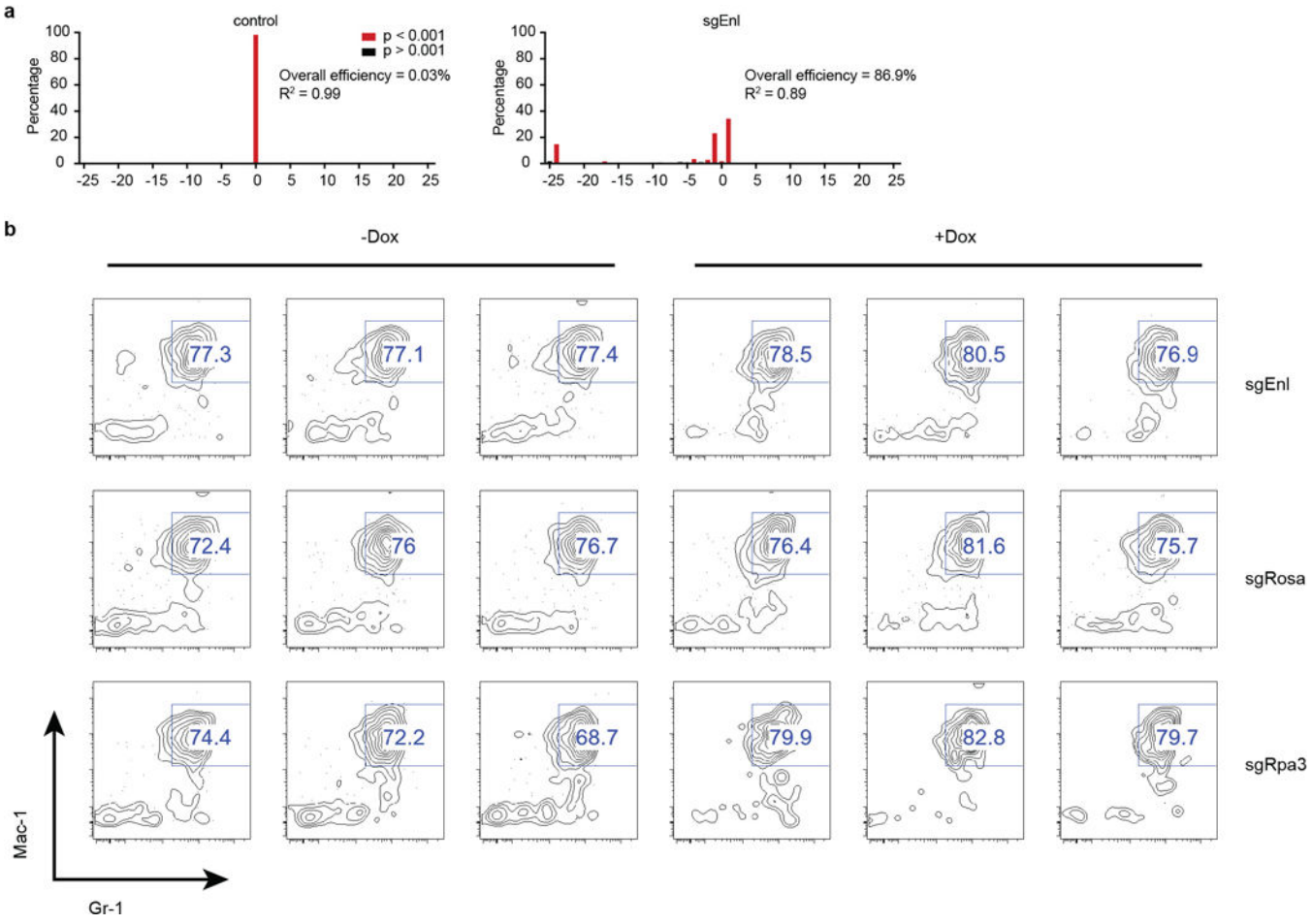

Extended Data Figure 2.

(a) Validation of sgRNA targeting mouse *Enl*. Indel quantification of genomic *Enl* locus in NIH/3T3-Cas9 cells by TIDE (tracking of indels by sequence trace decomposition) analysis 5 days after transduction with control sgRosa26 (left) or sgEnl (right).
(b) Mac-1and Gr-1 myeloid marker staining of viable dox-inducible Cas9-expressing LSK cells 9 days post-transduction with the sgRNA indicated.

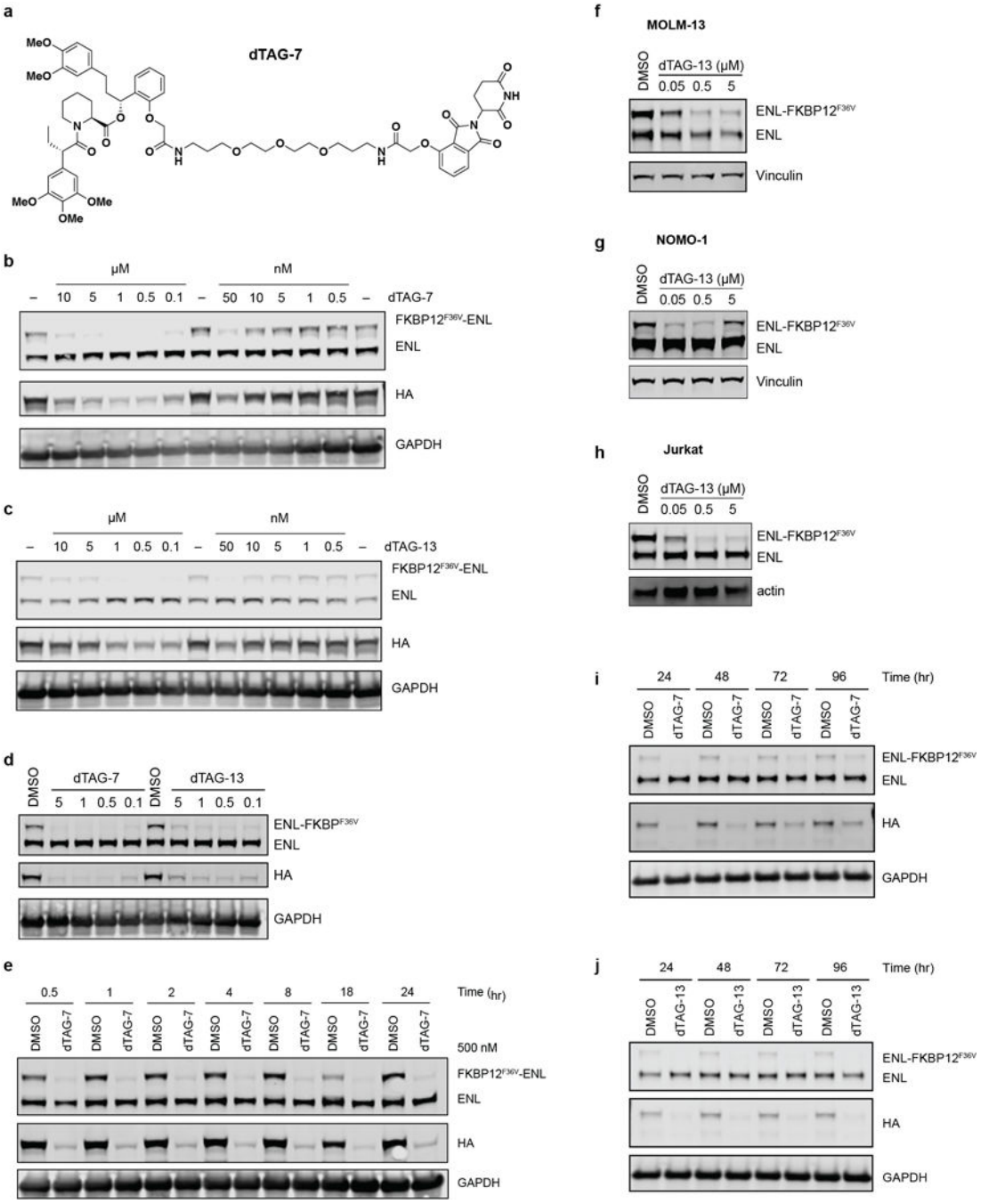

Extended Data Figure 3.
(a) Chemical structure of dTAG-7.

(b) Dose-responsive FKBP12^{F36V}-ENL degradation detected by immunoblot after 16 hour treatment of MV4;11 (Cas9+, FKBP12^{F36V}-HA-ENL+) cells with DMSO (labelled with "−") or dTAG-7 at the indicated concentration.
(c) As in (b), but with dTAG-13.
(d) Immunoblot detection of ENL-FKBP12^{F36V} degradation in MV4;11 (Cas9+, ENL-FKBP12^{F36V}-HA+) after 16 hours.
(e) Kinetic evaluation of FKBP12^{F36V}-ENL degradation by dTAG-7 (500 nM) in MV4;11 (Cas9+, FKBP12^{F36V}-HA-ENL+) cells.
(f) Degradation of ENL-FKBP12^{F36V} in MOLM-13 cells following a 4-hour treatment of ENL-FKBP12^{F36V}-expressing cells with dTAG-13 (500 nM).
(g) As in (f), but with NOMO-1 cells expressing ENL-FKBP12^{F36V}.
(h) As in (f), but with JURKAT cells expressing ENL-FKBP12^{F36V}.
(i) Long-term kinetic evaluation of ENL-FKBP12^{F36V} degradation by a single dose of dTAG-7 (500 nM) in MV4;11 (Cas9+, ENL-FKBP12^{F36V}-HA+) cells.
(j) As in (i), but with dTAG-13 (500 nM).

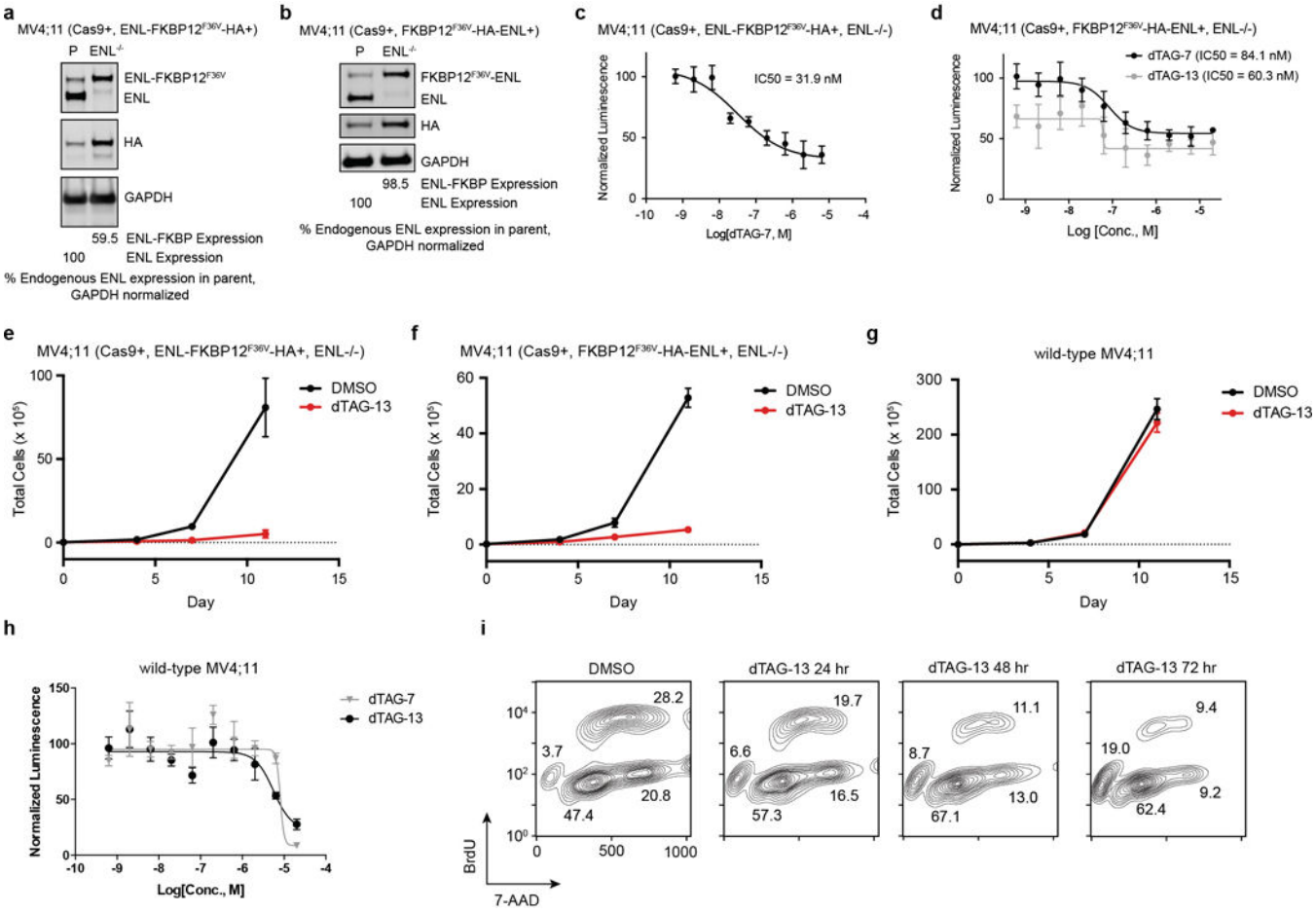

Extended Data Figure 4.

(a) CRISPR-Cas9 knockout of endogenous ENL in MV4;11 (Cas9+, ENL-FKBP12^{F36V}-HA+) cells. ENL/HA immunoblot in MV4;11 (Cas9+, ENL-FKBP12^{F36V}-HA+) (P, parental) and MV4;11 (Cas9+, ENL-FKBP12^{F36V}-HA+, ENL$^{-/-}$) cells.

(b) CRISPR-Cas9 knockout of endogenous ENL in MV4;11 (Cas9+, FKBP12^{F36V}-HA-ENL+) cells.

(c) DMSO-normalized cellular viability of MV4;11 (Cas9+, ENL-FKBP12^{F36V}-HA+, ENL$^{-/-}$) cells after 72-hour treatment with dTAG-13 approximated by ATP-lite assay (means ± s.d., $n = 4$).

(d) DMSO-normalized cellular viability of MV4;11 (Cas9+, FKBP12^{F36V}-HA-ENL+, ENL$^{-/-}$) cells after 72-hour treatment with dTAG-7 or dTAG-13 approximated by ATP-lite assay (means ± s.d., $n = 4$).

(e) Growth over time of MV4;11 (Cas9+, ENL-FKBP12^{F36V}-HA+, ENL$^{-/-}$) cells treated with DMSO or dTAG-13 (500 nM). Total number of viable cells as approximated by trypan blue exclusion is plotted over time (means ± s.d., $n = 3$).

(f–g) As in (e), but with cell line indicated at top.

(h) As in (d), but with wild-type MV4;11 cells.

(i) Representative plots of BrdU incorporation used for cell cycle analysis shown in Fig. 2f.

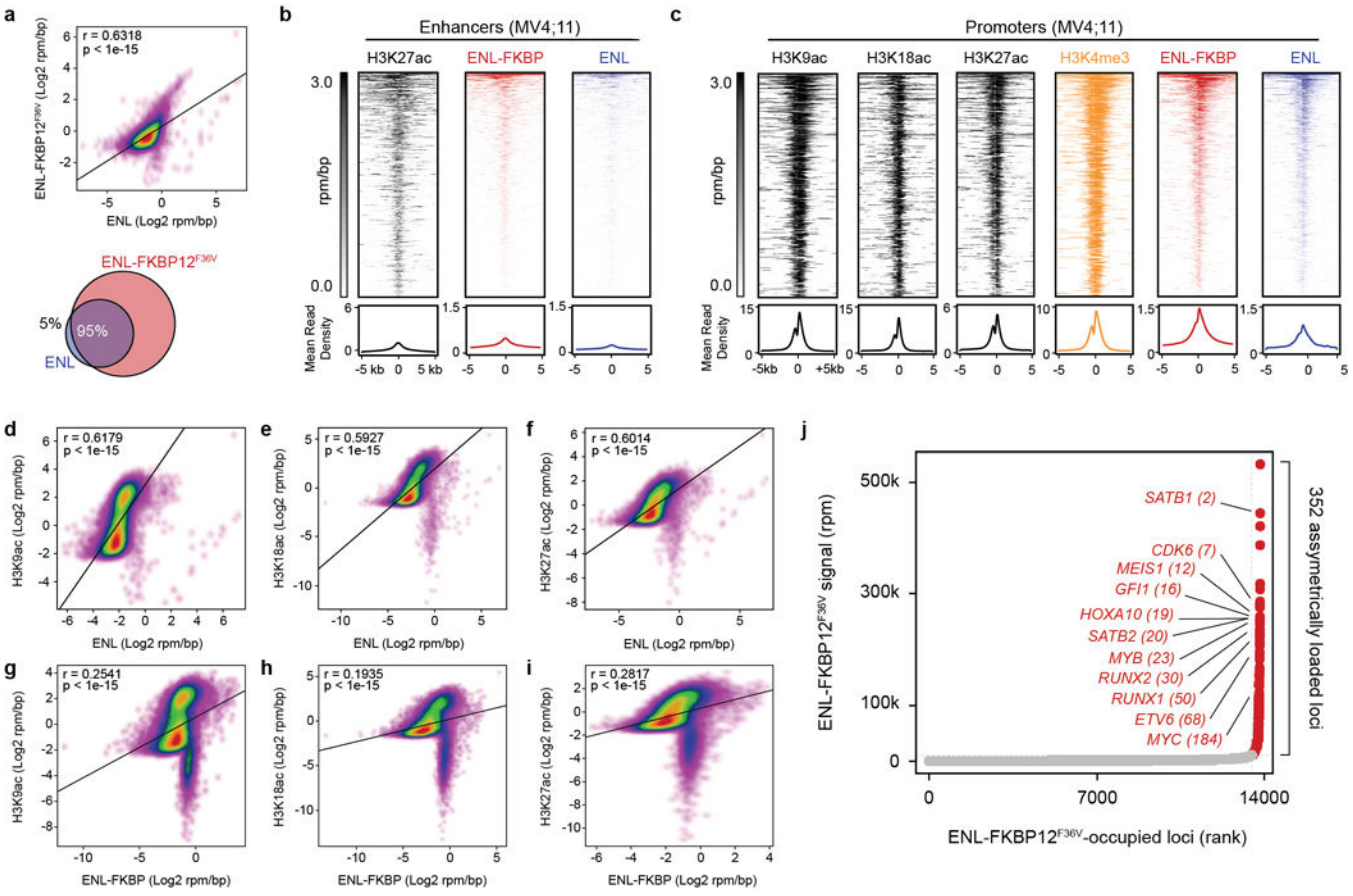

Extended Data Figure 5.

(a) Correlation of ENL and ENL-FKBP12^{F36V} genomic enrichment by ChIP-seq. Top: scatterplot of ENL-FKBP12^{F36V} and ENL ChIP-seq signal (log2 rpm/bp) at the union of all

regions enriched with ENL-FKBP12^{F36V} or ENL. Bottom: Venn diagram depicts the number of unique and overlapping regions of enrichment identified by ChIP-seq of ENL-FKBP12^{F36V} (18,294 total) and ENL (5,397 total).

(b) ENL binding at active enhancers. Top: Rank ordered heat map of H3K27ac, ENL-FKBP12^{F36V}, and ENL at H3K27ac-defined active enhancers. Rows depict a single enhancer (centered on an H3K27ac peak) and are sorted by ENL-FKBP12^{F36V} signal (rpm/bp). ChIP-seq signal (rpm/bp) is depicted by scaled color intensity. Bottom: meta plot representation of heat maps. Average read density is plotted against the distance from the enhancer center.

(c) ENL binding at promoters by ChIP-seq. Top: Rank ordered heat map of ChIP-seq signals at ENL-FKBP12^{F36V}-bound promoters, sorted by ENL-FKBP12^{F36V} levels and aligned at TSSs. ChIP-seq signal (rpm/bp) is depicted by scaled color intensity. Bottom: meta plot representation of heat maps. Average read density is plotted against the distance from the TSS. H3K9ac, ENL-FKBP12^{F36V}, and ENL samples are shown also in Fig. 3a.

(d–i) Correlation of ENL and ENL-FKBP12^{F36V} with histone acetyl-lysine residues by ChIP-seq. Scatterplot of ChIP-seq signals (log2 rpm/bp) at the union of all enriched regions for the two samples indicated in each plot.

(j) Asymmetric localization of ENL-FKBP12^{F36V}. ChIP-seq signal (rpm) at each location is plotted against its rank among all occupied regions. Points colored red are loci with asymmetric ENL-FKBP12^{F36V} load compared to typically loaded regions shown in gray. P-values determined by Pearson correlation.

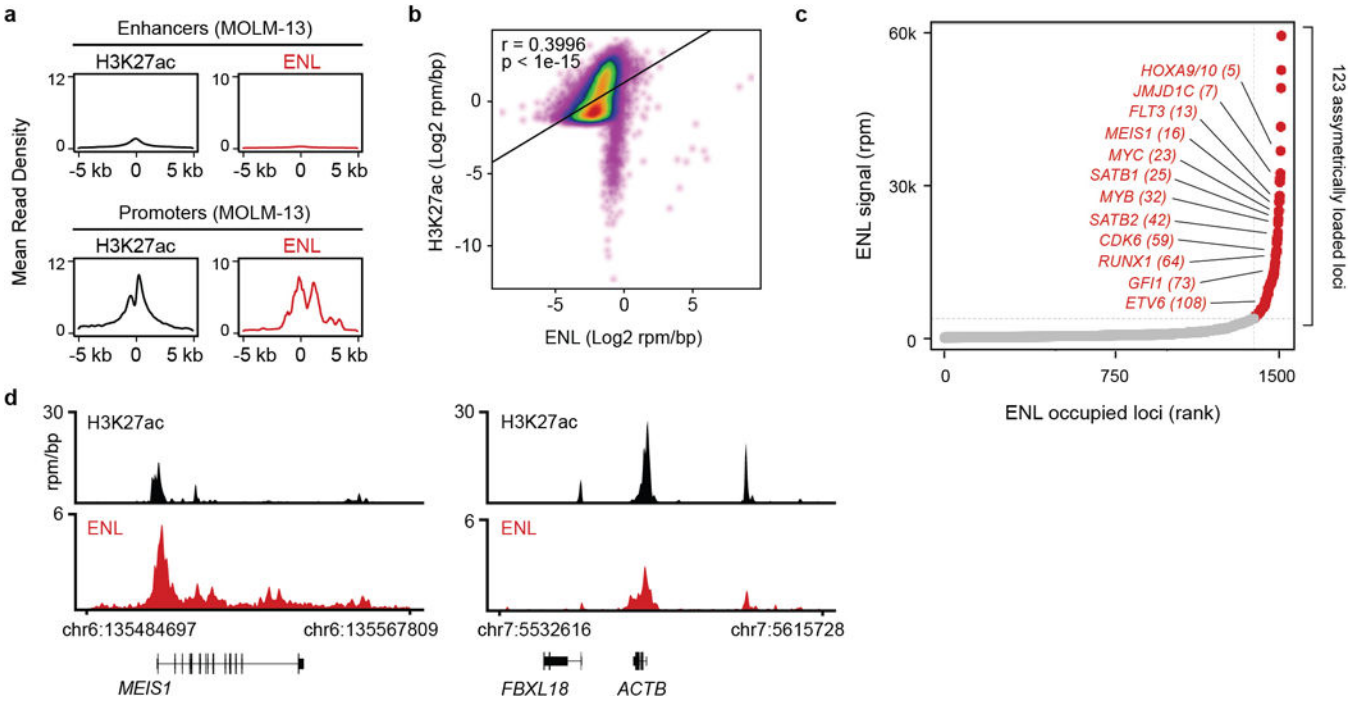

Extended Data Figure 6.

(a) ENL binding at enhancers and promoters. Top: Mean H3K27ac and ENL ChIP-seq signal across all H3K27ac-defined active enhancers in MOLM-13 cells. Average read density is plotted against the distance from the enhancer center. Bottom: Mean H3K27ac and

ENL ChIP-seq signal at ENL-bound TSS regions in MOLM-13 cells. Average read density is plotted against the distance from the TSS. Dataset for H3K27ac was obtained from GEO ID: GSM1652920.

(b) Correlation of H3K27ac and ENL genomic enrichment by ChIP-seq. Scatterplot of H3K27ac and ENL ChIP-seq signal (log2 rpm/bp) at the union of all H3K27ac and ENL enriched regions genome-wide. P-value determined by Pearson correlation.

(c) Asymmetric localization of ENL in MOLM-13 cells. ChIP-seq signal (rpm) at each location is plotted against its rank among all occupied regions. Points colored red are loci with asymmetric ENL load compared to typically loaded regions shown in gray.

(d) Gene tracks of ChIP-seq signal (rpm/bp) at examples of asymmetrically (*MYB*) and typically enriched ENL target genes (*ACTB*).

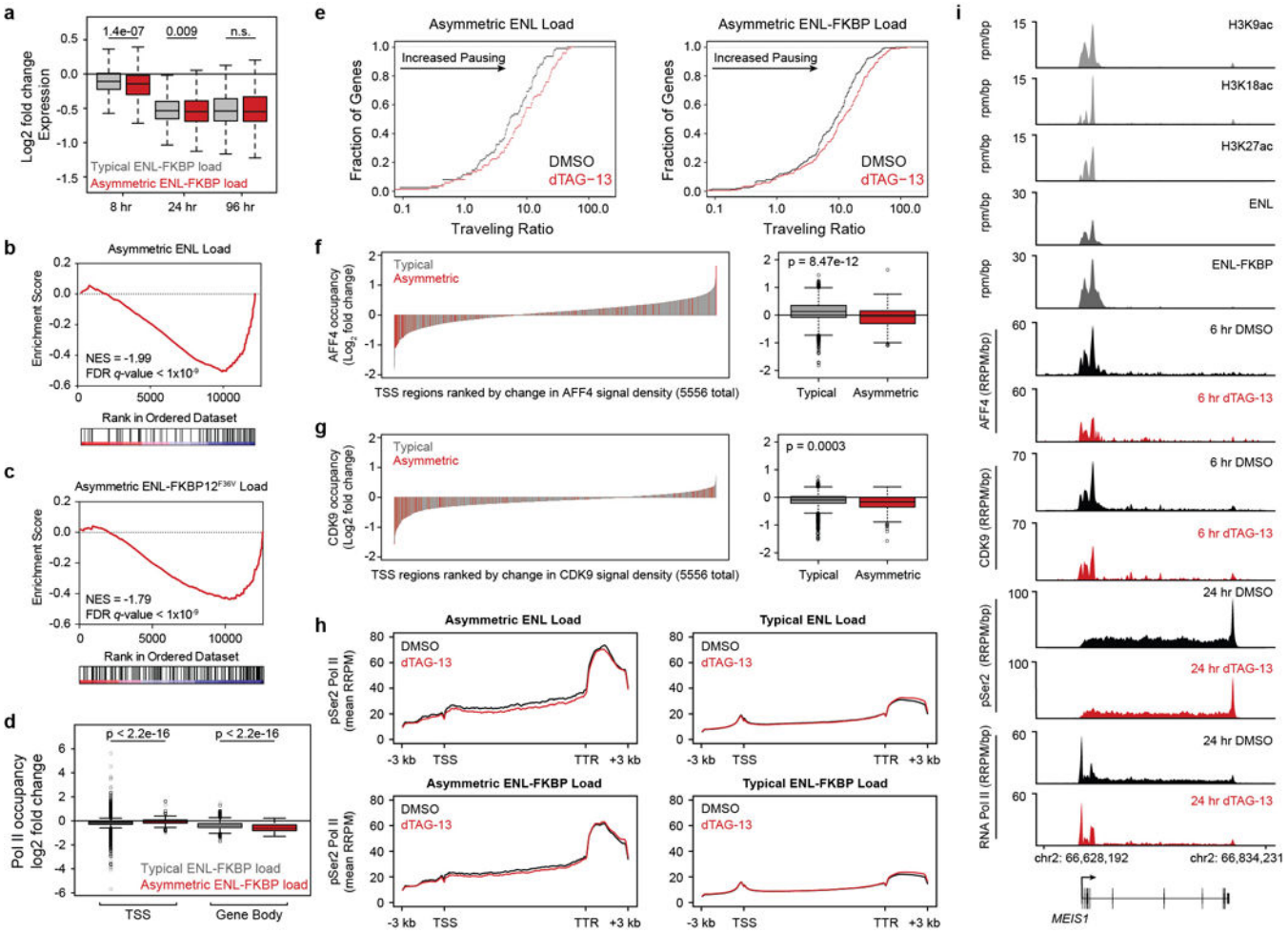

Extended Data Fig 7.

(a) Boxplot of DMSO-normalized fold changes in gene expression of typically enriched (gray) and asymmetrically enriched (red) ENL-FKBP12^{F36V} target genes with dTAG-13 (500 nM) treatment. Welch's two-tailed t-test *p*-values are indicated at top.

(b–c) Gene set enrichment analysis (GSEA) of DMSO normalized gene-expression changes with 8-hour dTAG-13 (500 nM) treatment compared to the set of asymmetrically loaded ENL (b) and ENL-FKBP12^{F36V} (c) target genes.

(d) Boxplots of change in RNA Pol II ChIP-Rx signal (RRPM) at TSS and gene-body regions of typically enriched (gray) and asymmetrically enriched (red) ENL-FKBP12^{F36V} target genes following 24 hour dTAG-13 (500 nM) treatment. Welch's two-tailed t-test *p*-values are indicated at top.

(e) Cumulative distribution plot of RNA Pol II traveling ratio at asymmetrically loaded ENL (left) and ENL-FKBP12^{F36V} (right) target genes determined by RNA Pol II ChIP-Rx following 24 hour DMSO or dTAG-13 (500 nM) treatment.

(f) Left: Waterfall plot of change in AFF4 ChIP-Rx signal (RRPM) at promoters (TSS ± 5 kb) of ENL-FKBP12^{F36V} target genes (typically enriched in gray, asymmetrically enriched in red) following dTAG-13 (500 nM treatment) for 6 hours. Right: boxplot of (left) with Welch's two-tailed t-test *p*-values indicated at top.

(g) As in (f), but for CDK9

(h) Meta-gene representations of pSer2-RNA Pol II ChIP-Rx signal at ENL and ENL-FKBP12^{F36V} target genes following 24 hour dTAG-13 (500 nM) treatments. TSS, Transcription start site; TTR, transcription termination region.

(i) Gene tracks of ChIP-seq signal (rpm/bp or RRPM/bp) at an example of an asymmetrically enriched ENL target gene, *MEIS1*.

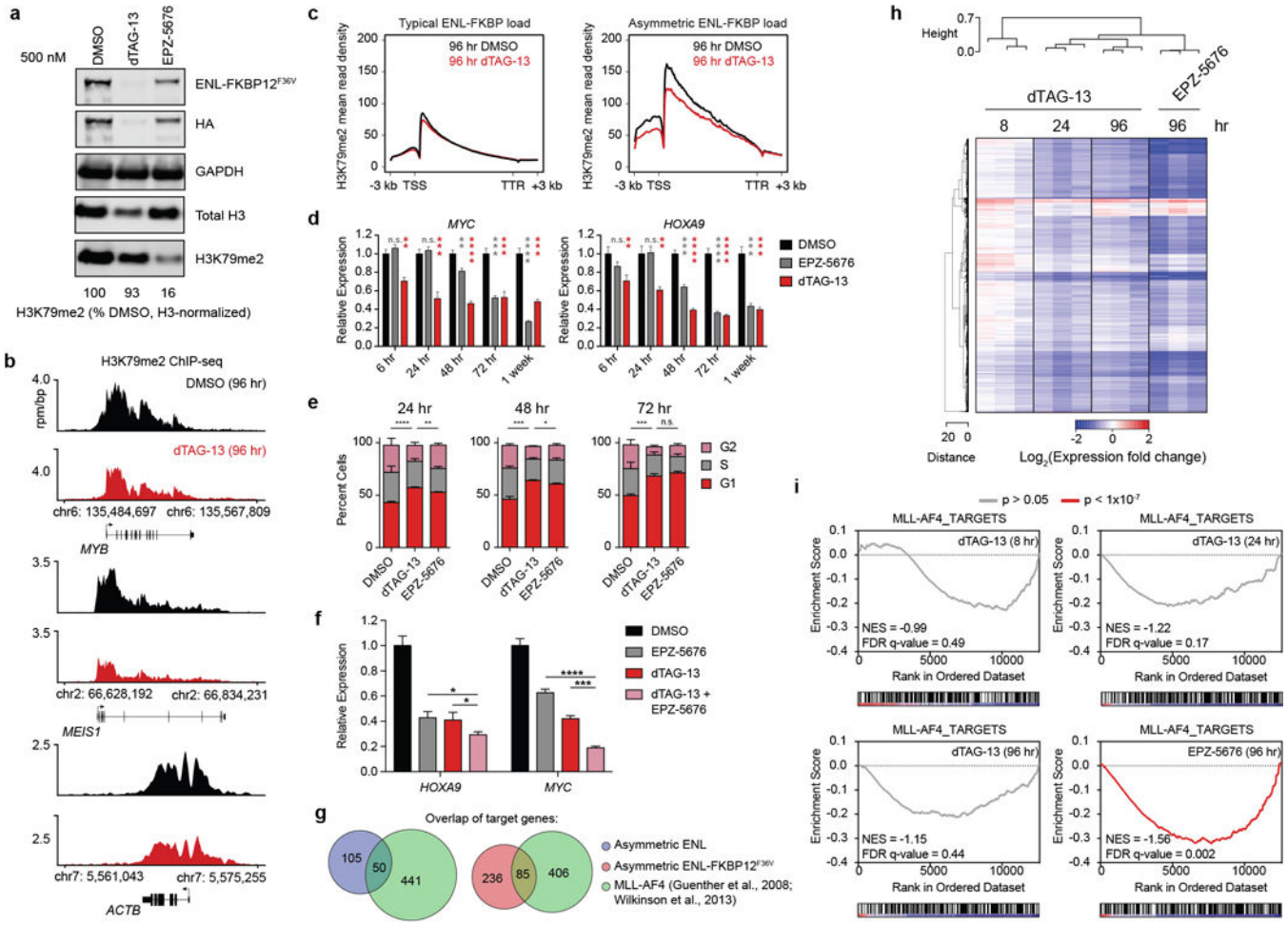

Extended Data Fig 8.

(a) Immunoblot for H3K79me2 following 96 hour DMSO, dTAG-13 (500 nM), or EPZ-5676 (500 nM) treatment. Bottom: semi-quantitative representation of H3-normalized H3K79me2 signal as percent of DMSO treatment.

(b) Gene track view of H3K79me2 ChIP-seq signal (rpm/bp) at examples of ENL target genes (asymmetric load: *MYB* and *MEIS1*; typical load: *ACTB*) following 96 hour DMSO or dTAG13 (500 nM) treatments.

(c) Meta gene representation of H3K79me2 ChIP-seq mean read density at typically loaded (left) and asymmetrically loaded (right) ENL target genes.

(d) Kinetic comparison of dTAG-13 (500 nM) and EPZ-5676 (500 nM) on gene expression changes in MV4;11 (Cas9+, ENL-FKBP12^{F36V}-HA+, ENL$^{-/-}$) cells. Gene expression quantified by qRT-PCR (ddC$_t$ method). Student's t-tests comparing DMSO to EPZ-5676 and dTAG-13 are in gray and red, respectively. **** p-value < 0.0001, *** p-value < 0.001, ** p-value < 0.01, * p-value < 0.05, n.s. p-value > 0.05 (mean ± s.d., triplicate PCR analysis).

(e) Cell cycle analysis via propidium iodide staining of MV4;11 (Cas9+, ENL-FKBP12^{F36V}-HA+, ENL$^{-/-}$) cells treated with DMSO, dTAG-13 (500 nM), or EPZ-5676 (500 nM). Percentage of G1 cells were compared by two-tailed t-tests: **** p-value <

0.0001, *** p-value < 0.001, ** p-value < 0.01, * p-value < 0.05, n.s. p-value > 0.05 (mean ± s.d., $n = 3$).

(f) Gene expression changes in MV4;11 (Cas9+, ENL-FKBP12^{F36V}-HA+, ENL$^{-/-}$) cells with combination treatments of dTAG-13 (500 nM) and EPZ-5676 (500 nM). Gene expression quantified by qRT-PCR (ddC_t method). Student's t-test: **** p-value < 0.0001, *** p-value < 0.001, ** p-value < 0.01, * p-value < 0.05, n.s. p-value > 0.05 (mean ± s.d., triplicate PCR analysis).

(g) Overlap analysis of published MLL-AF4 target genes and asymmetrically loaded ENL or ENL-FKBP12 target genes.

(h) Heat map of DMSO normalized fold changes in gene expression caused by dTAG-13 (500 nM) or EPZ-5676 (500 nM) treatment for the indicated amount of time. Raw expression values determined by RNA-seq were cell count normalized by spike-in of synthetic ERCC RNA standards. dTAG-13 data is redundant with data shown in Fig. 2g.

(i) GSEA of DMSO normalized gene-expression changes with dTAG-13 (500 nM) or EPZ-5676 (500 nM) treatment compared to MLL-AF4 target genes.

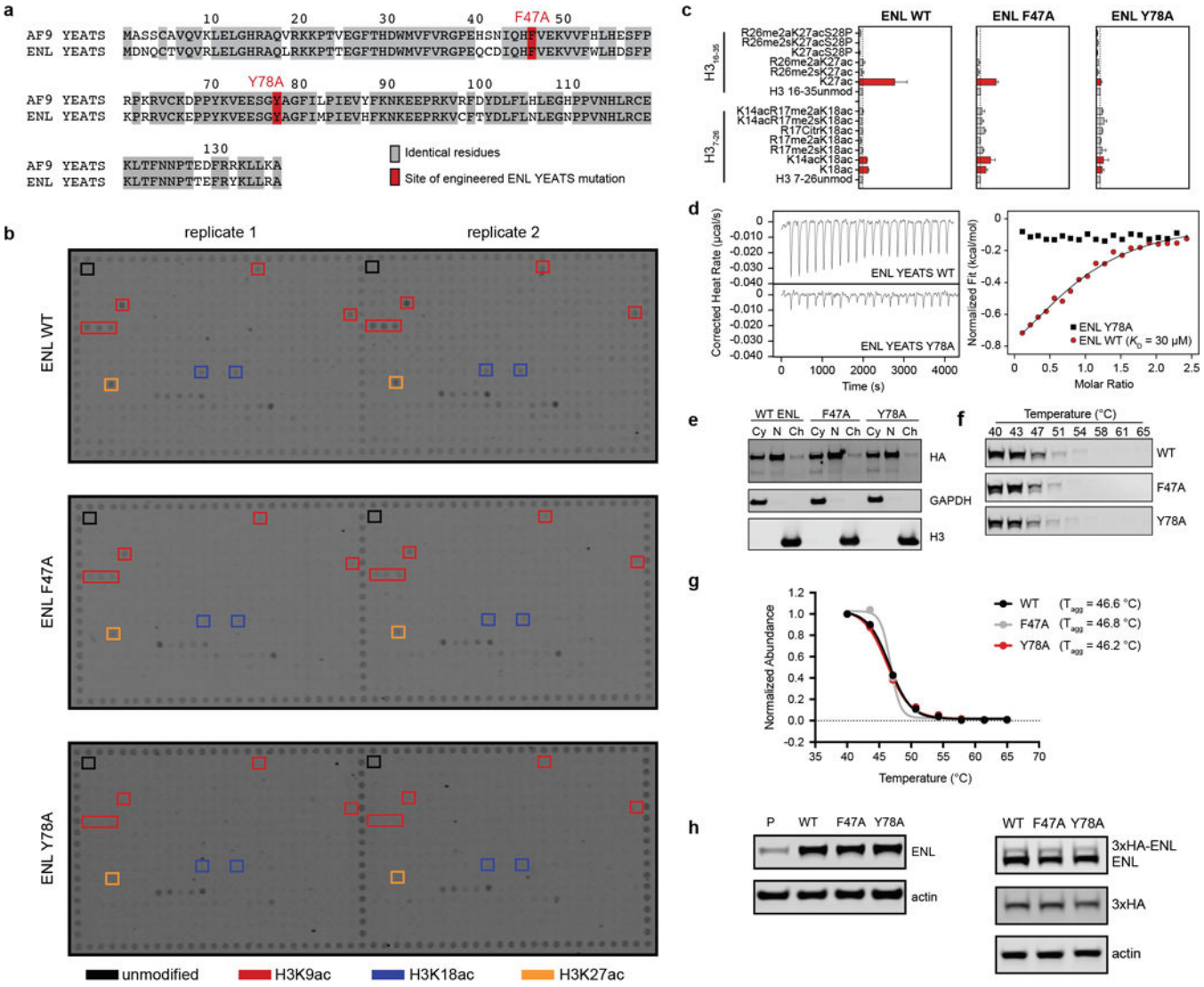

Extended Data Figure 9.

(a) Sequence alignment of AF9 and ENL YEATS domains. Identical residues are highlighted in gray. Two of these residues are colored red to denote sites where mutations were engineered into ENL for interrogation of YEATS function.

(b) Histone peptide microarray probed with lysates from 293T cells overexpressing full-length ENL WT, F47A, or Y78A with a 3xHA epitope tag. Select residues known to be YEATS domain substrates and showing YEATS domain dependent signal have been boxed in red, blue, or orange. Several other spots showed high signal, but not enriched over the corresponding unmodified peptide, and not YEATS-dependent. These have not been boxed in.

(c) Quantification of histone peptide microarray spots containing H3K18ac or H3K27ac after probing with cellular lysates from 293T cells overexpressing wild-type or mutant 3xHA-ENL. Mean ± s.d., $n = 2$.

(d) Isothermal titration calorimetry (ITC) measurements showing wild type ENL bound to H3(4-10)K9ac in a 1:0.943 stoichiometry with binding affinity (K_D) of 30.1 uM. Interaction was not detected with ENL Y78A.

(e) Subcellular localization of ENL. MV4;11 cells stably expressing 3xHA-ENL (wild-type, F47A, or Y78A) were fractionated and probed by immunoblot. Cy, cytoplasm; N, nucleoplasm; Ch, chromatin.

(f) Thermal stability of ENL in cells. MV4;11 cells stably expressing 3xHA-ENL (wild-type, F47A, or Y78A) were heated to the indicated temperature to induce irreversible aggregation. Remaining soluble protein was isolated and probed by immunoblot.

(g) Quantification of band intensity in from (e) showing the temperature of aggregation (T_{agg}).

(h) Immunoblot to determine expression level of exogenously expressed ENL constructs used for rescue and ChIP-qPCR experiments.

Supplementary Material

Refer to Web version on PubMed Central for supplementary material.

Acknowledgments

The authors thank S.A. Armstrong, C.D. Allis, and X. Shi for transparent and supportive dialogue. We also thank J.A. Perry for editing the manuscript and N.S. Gray and C.J. Ott for helpful suggestions. Quantitative proteomics studies were performed by R. Kunz of the TCMP at Harvard Medical School. This research was supported by philanthropic gifts from Kate Lubin and Emily Woods, as well as NIH grants (R01-CA176745 and P01-CA109901 to J.E.B.). G.E.W. was supported by an EMBO long-term fellowship. D.L.B. is a Merck Fellow of the Damon Runyon Cancer Research Foundation (DRG-2196-14). N.E.S. is supported by a Pathway to Independence Award (R00-HG008171) from the NHGRI.

References

1. Krivtsov AV, Armstrong SA. MLL translocations, histone modifications and leukaemia stem-cell development. Nat Rev Cancer. 2007; 7:823–833. [PubMed: 17957188]
2. Slany RK. When epigenetics kills: MLL fusion proteins in leukemia. Hematol Oncol. 2005; 23:1–9. [PubMed: 16118769]
3. Cai SF, Chen CW, Armstrong SA. Drugging Chromatin in Cancer: Recent Advances and Novel Approaches. Molecular Cell. 2015; 60:561–570. [PubMed: 26590715]
4. Ott CJ, et al. BET bromodomain inhibition targets both c-Myc and IL7R in high-risk acute lymphoblastic leukemia. Blood. 2012; 120:2843–2852. [PubMed: 22904298]
5. Delmore JE, et al. BET bromodomain inhibition as a therapeutic strategy to target c-Myc. Cell. 2011; 146:904–917. [PubMed: 21889194]
6. Zuber J, et al. RNAi screen identifies Brd4 as a therapeutic target in acute myeloid leukaemia. Nature. 2011; 478:524–528. [PubMed: 21814200]
7. Bernt KM, et al. MLL-Rearranged Leukemia Is Dependent on Aberrant H3K79 Methylation by DOT1L. Cancer Cell. 2011; 20:66–78. [PubMed: 21741597]
8. Daigle SR, et al. Potent inhibition of DOT1L as treatment of MLL-fusion leukemia. Blood. 2013; 122:1017–1025. [PubMed: 23801631]
9. Daigle SR, et al. Selective Killing of Mixed Lineage Leukemia Cells by a Potent Small-Molecule DOT1L Inhibitor. Cancer Cell. 2011; 20:53–65. [PubMed: 21741596]
10. Guenther MG, et al. Aberrant chromatin at genes encoding stem cell regulators in human mixed-lineage leukemia. Genes & Development. 2008; 22:3403–3408. [PubMed: 19141473]
11. Krivtsov AV, et al. H3K79 Methylation Profiles Define Murine and Human MLL-AF4 Leukemias. Cancer Cell. 2008; 14:355–368. [PubMed: 18977325]

12. Okada Y, et al. hDOT1L Links Histone Methylation to Leukemogenesis. Cell. 2005; 121:167–178. [PubMed: 15851025]
13. Shalem O, et al. Genome-scale CRISPR-Cas9 knockout screening in human cells. Science. 2014; 343:84–87. [PubMed: 24336571]
14. Luo B, et al. Highly parallel identification of essential genes in cancer cells. Proc Natl Acad Sci USA. 2008; 105:20380–20385. [PubMed: 19091943]
15. Levis M, et al. A FLT3-targeted tyrosine kinase inhibitor is cytotoxic to leukemia cells in vitro and in vivo. Blood. 2002; 99:3885–3891. [PubMed: 12010785]
16. Wang T, et al. Identification and characterization of essential genes in the human genome. Science. 2015; 350:1096–1101. [PubMed: 26472758]
17. Li Y, et al. AF9 YEATS Domain Links Histone Acetylation to DOT1L-Mediated H3K79 Methylation. Cell. 2014; 159:558–571. [PubMed: 25417107]
18. Li Y, et al. Molecular Coupling of Histone Crotonylation and Active Transcription by AF9 YEATS Domain. Molecular Cell. 2016; 62:181–193. [PubMed: 27105114]
19. Andrews FH, et al. The Taf14 YEATS domain is a reader of histone crotonylation. Nat Chem Biol. 2016; 12:396–398. [PubMed: 27089029]
20. Shanle EK, et al. Association of Taf14 with acetylated histone H3 directs gene transcription and the DNA damage response. Genes & Development. 2015; 29:1795–1800. [PubMed: 26341557]
21. Mueller D, et al. A role for the MLL fusion partner ENL in transcriptional elongation and chromatin modification. Blood. 2007; 110:4445–4454. [PubMed: 17855633]
22. Yokoyama A, Lin M, Naresh A, Kitabayashi I, Cleary ML. A Higher-Order Complex Containing AF4 and ENL Family Proteins with P-TEFb Facilitates Oncogenic and Physiologic MLL-Dependent Transcription. Cancer Cell. 2010; 17:198–212. [PubMed: 20153263]
23. He N, et al. Human Polymerase-Associated Factor complex (PAFc) connects the Super Elongation Complex (SEC) to RNA polymerase II on chromatin. Proc Natl Acad Sci USA. 2011; 108:E636–45. [PubMed: 21873227]
24. Rubnitz JE, Morrissey J, Savage PA, Cleary ML. ENL, the gene fused with HRX in t(11;19) leukemias, encodes a nuclear protein with transcriptional activation potential in lymphoid and myeloid cells. Blood. 1994; 84:1747–1752. [PubMed: 8080983]
25. Zeisig DT, et al. The eleven-nineteen-leukemia protein ENL connects nuclear MLL fusion partners with chromatin. Oncogene. 2005; 24:5525–5532. [PubMed: 15856011]
26. Winter GE, et al. Phthalimide conjugation as a strategy for in vivo target protein degradation. Science. 2015; 348:1376–1381. [PubMed: 25999370]
27. Clackson T, et al. Redesigning an FKBP-ligand interface to generate chemical dimerizers with novel specificity. Proc Natl Acad Sci USA. 1998; 95:10437–10442. [PubMed: 9724721]
28. Rathert P, et al. Transcriptional plasticity promotes primary and acquired resistance to BET inhibition. Nature. 2015; 525:543–547. [PubMed: 26367798]
29. Wilkinson AC, et al. RUNX1 Is a Key Target in t(4;11) Leukemias that Contributes to Gene Activation through an AF4-MLL Complex Interaction. CellReports. 2013; 3:116–127.
30. Shi J, et al. Discovery of cancer drug targets by CRISPR-Cas9 screening of protein domains. Nat Biotechnol. 2015; 33:661–667. [PubMed: 25961408]
31. Peterlin BM, Price DH. Controlling the elongation phase of transcription with P-TEFb. Mol Cell. 2006; 23:297–305. [PubMed: 16885020]

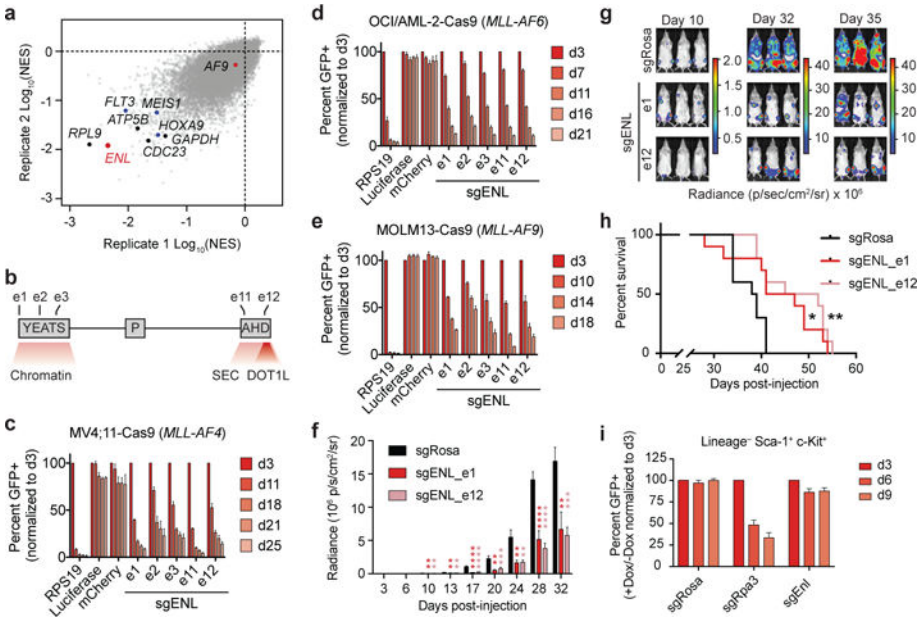

Figure 1. ENL is required for growth of acute leukemia

(a) RIGER analysis (normalized enrichment score, NES) of pooled CRISPR/Cas9 screen in MV4;11 cells. Select essential and leukemic driver genes are shown in black and blue, respectively.

(b) Schematic depiction of ENL domain structure: YEATS, polyproline region (P), and AHD (Anc1 homology domain). Numbering indicates sgRNA exon targets in (c-e).

(c–e) Competition-based CRISPR-Cas9 mutagenesis assays. GFP+ (sgRNA+) subpopulation percentage is depicted for the indicated day after lentiviral transduction. Mean ± s.d., $n = 3$.

(f) Luminescence of MV4;11 (Cas9+, Luciferase+) cells in a disseminated model of leukemia at the indicated day after xenotransplantation. sgRosa denotes a control sgRNA targeting the mouse Rosa26 locus (non-targeting in human cells). P values obtained via two-tailed Student's t-tests, comparing each ENL sgRNA against the Rosa26 sgRNA. Mean ± s.e.m., $n = 10$.

(g) Representative images of mice from (f). The same mice are depicted at each time-point.

(h) Kaplan–Meier plot for overall survival of mice from (f). $n = 10$, p-value obtained from Mantel-Cox test.

(i) Competition-based CRISPR-Cas9 mutagenesis in LSK cells. Percent GFP+ (sgRNA+) after doxycycline induction of Cas9 expression. Mean ± s.d., $n = 3$.

**** p-value < 0.0001, *** p-value < 0.001, ** p-value < 0.01, * p-value < 0.05.

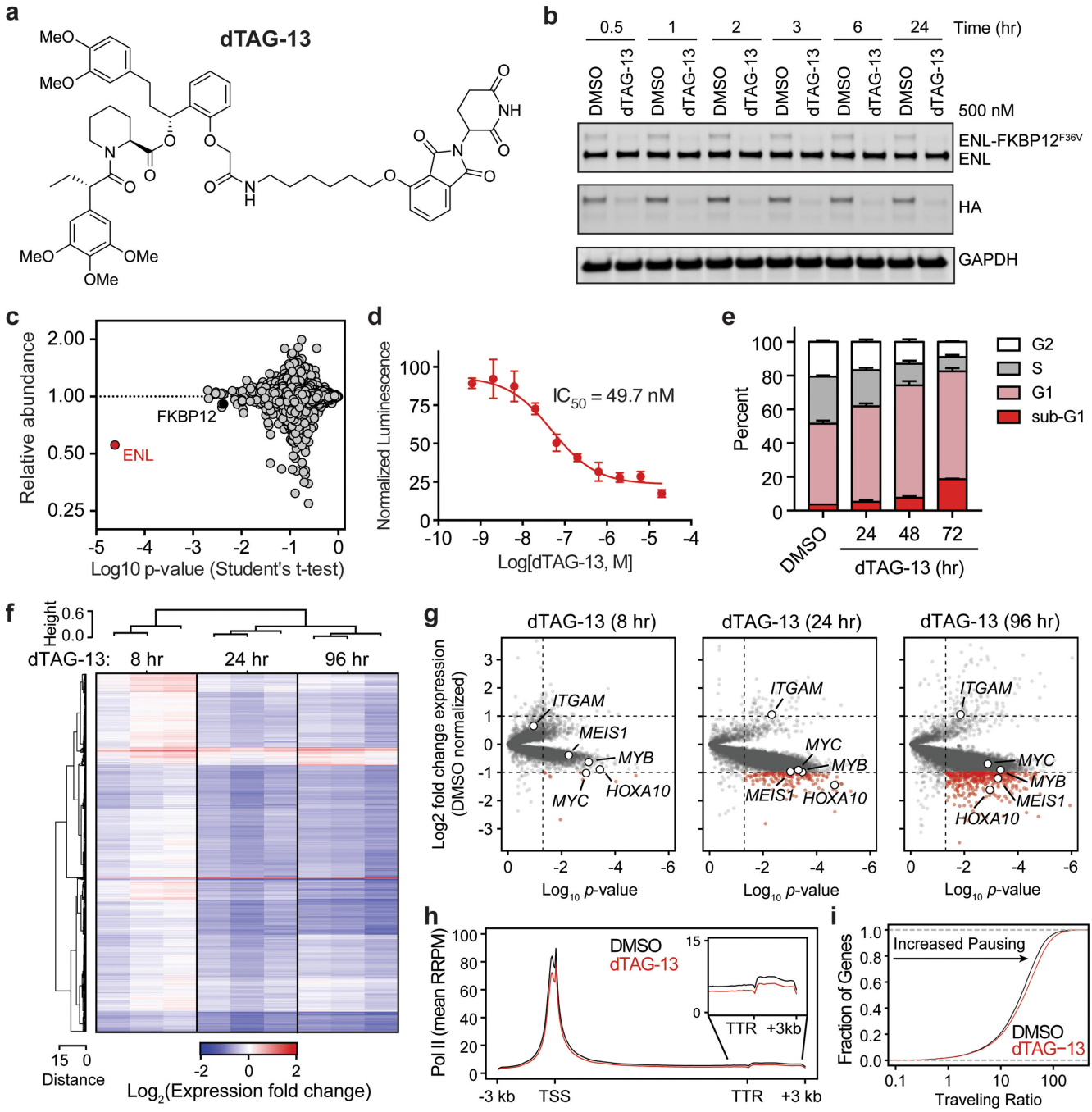

Figure 2. ENL degradation induces growth arrest and transcription defects genome-wide

(a) Chemical structure of dTAG-13.

(b) Kinetic evaluation of ENL-FKBP12^{F36V} degradation in MV4;11 (Cas9+, ENL-FKBP12^{F36V}-HA+) cells.

(c) Quantification of protein abundance following a 3 hour dTAG-13 treatment (500 nM) in MV4;11 (Cas9+, ENL-FKBP12^{F36V}-HA+, ENL−/−) cells for proteins with 3 or more quantified spectral counts, $n = 3$.

(d) DMSO-normalized cellular viability in MV4;11 (Cas9+, ENL-FKBP12^{F36V}-HA+) cells after 72-hour treatment with dTAG-13 approximated by ATP-lite assay. Mean ± s.d., $n = 4$.
(e) Cell cycle analysis with DMSO or dTAG-13 (500 nM) treatment by BrdU incorporation. Mean ± s.d., $n = 3$.
(f) Heat map representation of DMSO-normalized fold changes in cell-count normalized gene expression values caused by dTAG-13 (500 nM).
(g) Volcano plot of data shown in (f). *P*-value derived from two-tailed Student's t-test, $n = 3$.
(h) Meta gene representation of cell-count normalized ChIP-seq (ChIP-Rx) of RNA Pol II at active genes following DMSO or dTAG-13 (500 nM) treatment for 24 hours. TSS, Transcription start site; TTR, transcription termination region.
(i) Cumulative distribution plot of RNA Pol II traveling ratios from data shown in (h).

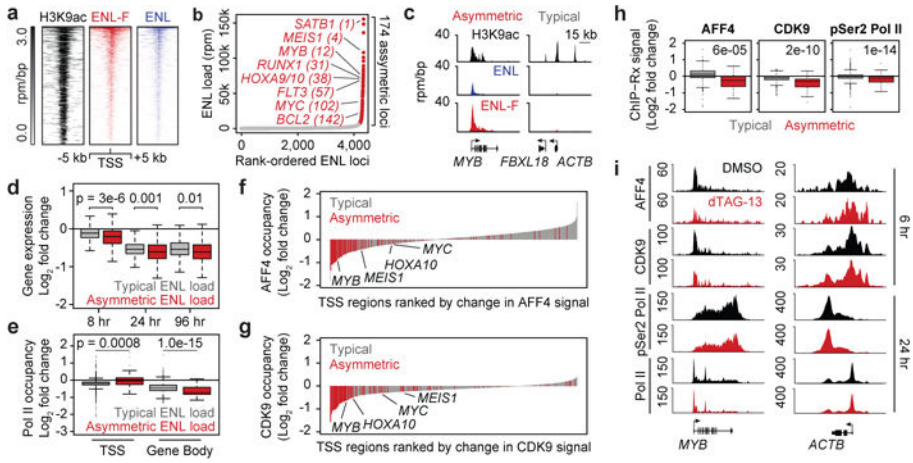

Figure 3. ENL degradation attenuates SEC recruitment and activity

(a) ENL promoter localization. Top: Rank ordered heat map of H3K9ac, ENL-FKBP12^{F36V}, and ENL ChIP-seq signal (rpm/bp) at ENL-FKBP12^{F36V}-bound promoters, sorted by ENL-FKBP12^{F36V} signal.

(b) Asymmetric localization of ENL. ENL ChIP-seq signal (rpm) at each location is plotted against its rank among all ENL-occupied regions. Red depicts asymmetrically loaded loci.

(c) Gene tracks of ChIP-seq signal (rpm/bp) at examples of asymmetrically and typically enriched ENL target genes.

(d) Boxplot of DMSO-normalized fold change in cell-count normalized RNA-seq values following dTAG-13 (500 nM) treatment.

(e) Boxplots of DMSO-normalized fold change in RNA Pol II ChIP-Rx signal following 24 hour dTAG-13 (500 nM) treatment.

(f) Waterfall plot of change in AFF4 ChIP-Rx signal at promoters (TSS ± 5 kb) of ENL target genes (2303 total) following dTAG-13 (500 nM) treatment for 6 hours.

(g) As in (f), but for CDK9 ChIP-Rx.

(h) Boxplots of change in ChIP-Rx signal for AFF4 and CDK9 at promoters (TSS ± 5 kb) and pSer2 at gene bodies of ENL target genes following dTAG-13 (500 nM) treatment (6 hr for AFF4 and CDK9, 24 hr for pSer2-RNAPII).

(i) Gene tracks of ChIP-Rx signal (RRPM/bp) at examples of asymmetrically and typically enriched ENL target genes.

P-values are indicated at top of boxplots (Welch's two-tailed t-tests).

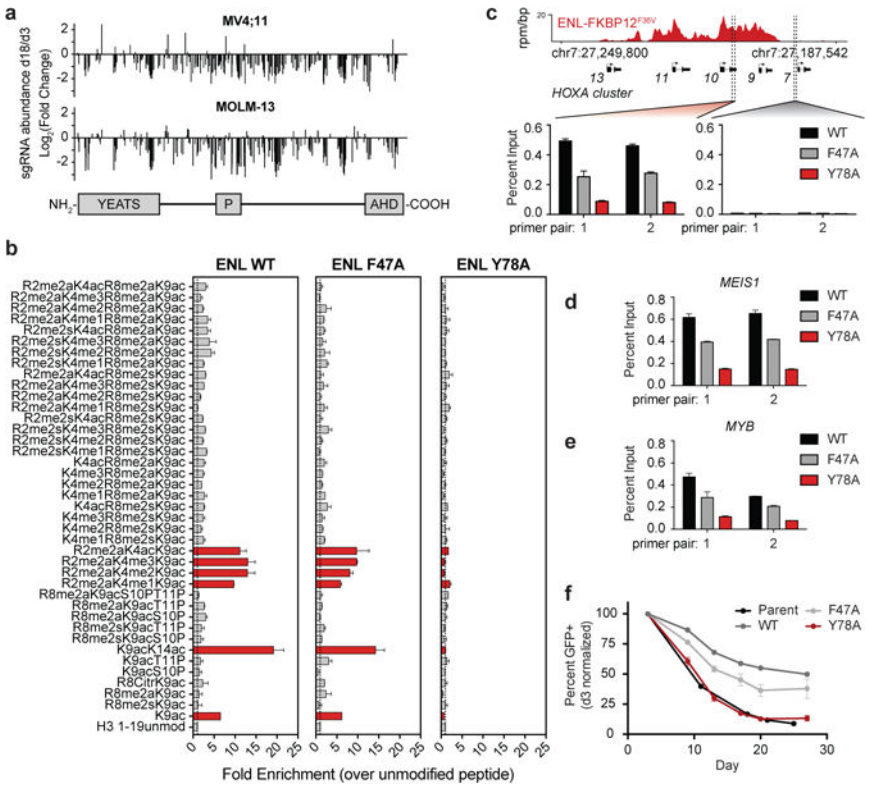

Figure 4. The YEATS domain is essential for ENL-dependent leukemic growth

(a) Scanning mutagenesis of ENL by pooled CRISPR/Cas9 targeting of all exonic PAMs for competitive growth assays.

(b) Quantification of histone peptide microarray spots containing H3K9ac after probing with cellular lysates from 293T cells overexpressing wild-type or mutant 3xHA-ENL. Mean ± s.d., $n = 2$.

(c) YEATS-dependent chromatin localization of ENL. Top: gene track view of ENL-FKBP12^{F36V} ChIP-seq signal. Bottom: ChIP-qPCR signal at the indicated locus by 2 independent primer pairs. Mean ± s.d., triplicate PCR analysis.

(d–e) As in (c), but for the the 5′ region of the indicated gene. Mean ± s.d., triplicate PCR analysis.

(f) Rescue of endogenous ENL loss by exogenous expression of wild-type and mutant *ENL*. The GFP+ (endogenous ENL-targeted sgRNA+) subpopulation percentage is depicted for the indicated day after lentiviral transduction. Mean ± s.e.m., $n = 3$.